J Mater Sci: Mater Med (2008) 19:2503–2513
DOI 10.1007/s10856-008-3389-2

Development of two alginate-based wound dressings

Chih-Tung Chiu · Jui-Sheng Lee · Chi-Shung Chu · Yi-Pin Chang · Yng-Jiin Wang

Received: 9 September 2007 / Accepted: 18 January 2008 / Published online: 12 February 2008

Abstract Two types of new alginate-based wound dressings, Type-AP and Type-AE, were fabricated by the EDC-activated crosslinking of alginate with Polyethyleneimine and Ethylenediamine, respectively. As compared with the commercial non-woven wound dressing, Kaltostat®, both Type-AP and Type-AE dressings had higher degradation temperature, lower calcium content, and a sponge-like macroporous structure. In addition, these two alginate-based dressings had higher mechanical stress (12.37 ± 1.72 and 6.87 ± 0.5 MPa for Type-AP and -AE, respectively) and higher water vapor transmission rates (both about 3,500 g/m^2/day) than Kaltostat^R (0.87 ± 0.12 MPa and 2,538 g/m^2/day). Fibroblasts proliferated faster on these two newly developed wound dressings at a higher rate as compared with that on Kaltostat® dressing. The results of animal study showed that the wounds treated with either Type-AP or Type-AE dressings healed faster than Kaltostat® with less encapsulation of residuals by fibrous tissue and more neo-capillary formation. These two newly developed Type-AP and Type-AE porous wound dressings thus have great potential for clinical applications.

C.-T. Chiu · Y.-P. Chang · Y.-J. Wang (✉)
Institute of Biomedical Engineering, National Yang Ming University, No. 155, Sec. 2, Li-Nung St., Beitou District, Taipei 11221, Taiwan, ROC
e-mail: wang@ym.edu.tw

J.-S. Lee · C.-S. Chu
Department of Raw Materials and Yarn Formation Section, Taiwan Textile Research Institute, Tu-chen, Taipei, Taiwan, ROC

1 Introduction

Large-scale burns and surgical wounds often require treatments with temporary skin grafts, which could be gradually replaced by the regenerated skin tissues of the patients. The main functions from the temporary wound dressings are: reducing evaporative water loss, nurturing vascularization and assisting tissue regeneration at the interface of the dressing and the wound tissue [1–3].

A wide variety of wound dressings are developed using biological polymers, and some of them are successful in various biomedical applications. Of the biopolymeric materials used, collagen, chitosan and alginate have been developed into clinical products. Collagen and chitosan both have contamination issues of pathogens and residual antibiotics. In contrast, alginate, which has excellent properties of biocompatibility, biodegradability and non-antigenicity, is considered as an alternative feasible material for constructing wound dressing [4].

Alginate, a polysaccharide from seaweed, is a linear biological copolymer consisting of (1 → 4) linked α-L-guluronate (G) and β-D-mannuronate (M) monomeric units. Alginate forms gel when it comes in contact with calcium ions [5, 6], and the resulted hydrogel has been widely investigated for use in many biotechnological and medical applications [7]. For example, sponge like alginate-based scaffolds have been designed to contain interconnecting macropores of ~100 μm. These scaffolds support the cultivation of a large cell mass as well as rearrange the dispersed cells into a functioning tissue, and therefore interact closely with the surrounding host tissue after implantation [8–10].

Choi et al. [11] prepared gelatin-alginate sponge wound dressings by various crosslinking methods. Crosslinking alginate with selected polymers increases the mechanical

strength and decreases the degradation rate of the alginate-based dressing [11, 12].

In order to synthesize alginate-based wound dressings with a slower degradation rate, we have fabricated two porous dressings made from composites of alginate-Polyethyleneimine (Type-AP) and alginate-Ethylenediamine (Type-AE); both of them were crosslinked with 1-ethyl-3-dimethylaminopropyl carbodiimide (EDC). In this study, these two dressings were characterized and their performances were compared with the commercial Kaltostat® (CV laboratories Ltd, Aldershot, Hants, UK), a non-woven fabric wound dressing composed of sodium calcium alginate fibers.

2 Materials and methods

High viscosity sodium alginate (MW: 80–120 K, M/G ratio = 1.56, 2% 3,500 cp 25°C), Polyethyleneimine (PEI), Ethylenediamine, sodium cacodylate, sodium calcium and 1-ethyl-3-dimethylaminopropyl carbodiimide (EDC) were all purchased from Sigma Company, St. Louis, MO. The PEI used in this study is a branched polymer with an average molecular weight of 25,000. Fetal calf serum and DMEM (Dulbecco's Modified Eagle Medium) were purchased from GIBCO BRL®, Glasgow, UK. All other reagents were purchased from Merck (Germany).

2.1 Preparation of alginate-based wound dressings

Sodium alginate powders were dissolved in double de-ionized water at 70°C to obtain a 1% (w/w) solution. This solution was used to fabricate the two alginate-based wound dressings, Type-AP (alginate-PEI) and Type-AE (alginate-Ethylenediamine). The fabrication procedures are described as below:

2.1.1 (i) Type-AP porous dressing

An aqueous solution containing 1% alginate, 1 mM PEI and 15 mM EDC was poured into a rectangular container (12 × 16 × 0.5 cm) and thoroughly mixed using a shaker at room temperature for 1 day. The container was then placed in an environmental chamber at −20°C overnight and lyophilized at −40°C (Virtis freezemobile 5SL, Gardiner, NY) for 3 days. The container contained the lyophilized alginate-PEI was next immersed in 100 mM $CaCl_2$ for 1 h, then washed with double de-ionized water 3 times (10 min each) and the aforementioned freeze-dry process was repeated to yield the final Type-AP porous dressing.

2.1.2 (ii) Type-AE porous dressing

This porous dressing was prepared the same as Type-AP except that the starting solution contained 1% alginate, 7.6 mM Ethylenediamine and 83.3 mM EDC.

2.2 IR spectra of the dressing materials

Freeze-dried sample of 10 mg was mixed with 300 mg dry KBr and pressed into a pellet using a macro KBr die kit. The solid pellet was analyzed by Fourier Transformed Infrared spectroscopy (FTIR) (Perkin-Elmer, PerkinElmer Life And Analytical Sciences, Inc., USA).

2.3 Scanning electron microscopic analysis of the dressings

The test sample was fixed with 2% glutaraldehyde in 0.1 M sodium cacodylate (pH 7.4), dehydrated with a series of ethanol solutions, and finally critical point dried with carbon dioxide. The dry sample was coated with a thin layer of gold (~30 nm) using an Agar Sputter Coater, and examined under a scanning electron microscope (SEM) equipped with an energy dispersive X-ray microanalyzer (Oxford ISIS 300 EDS, Inspiratech 2000 Ltd, UK).

2.4 Characterization of physical and chemical properties

The thermal properties of the test samples were analyzed using a Perkin–Elmer differential scanning calorimeter (DSC, Model DSC 7, Norwalk, Connecticut) with a temperature sweep from 20 to 400°C at a rate of 40°C/min.

For determining the moisture content, the sample was sandwiched between two paper towels and then a 40 g weight load was applied on the top for 10 s. The sample was first weighed (as the wet sample weight), and then lyophilized for 24 h and weighed to obtain its dry weight. The moisture content of the sample was calculated based on the following equation:

$$\text{Moisture content (\%)} = [(\text{wet sample weight} - \text{dry sample weight})/\text{wet sample weight}] \times 100\%.$$

To study their mechanical properties, samples were cut into 10 mm × 5 mm rectangles. The thickness was measured by a micrometer (Digimatic Micrometer MCD-25P, Mitutoyo, Tokyo, Japan). The tensile modulus and tensile failure strain were obtained by performing tensile tests of the samples on a universal testing machine (H1KS, Housfield, UK) with the strain rate of 2 mm/min.

The water vapor transmission rate (WVTR) was determined according to the desiccant method of the ASTM E96 [13]. Circular membranes of 15-mm diameter were each mounted onto a plastic container containing 19–20 g of activated silica gel and incubated at controlled environment of 32°C and 50% RH. The value of WVTR was calculated following the equation:

WVTR = W/(A * t), where W is the weight of water vapor transmitted through the membrane, A is the area (7.54 cm^2) of the membrane, and t is fixed at 24 h.

The amounts of free amine groups in the wound dressings were determined using the ninhydrin assay as previously described [14]. The test dressing was first lyophilized for 24 h and then weighed. Subsequently, the lyophilized test dressing was heated with a ninhydrin solution for 20 min. After reacting with ninhydrin, the optical absorbance of the solution at 570 nm was recorded with a spectrophometer (Model DU640B; Beckman-Coulter Inc.; California, USA) using ethylenediamine at various known concentrations as standard. It is known that the amount of free amino group in the test dressing, after heating with ninhydrin, is proportional to the optical absorbance of the solution.

2.5 Measurement of calcium ions

A total of 10 mg wound dressing sample was loaded into a test tube containing 10 ml of 0.9% (w/w) NaCl solution or DMEM physiological medium solution, which was then placed in a shaker at 2.5 Hz at 37°C. The calcium ions released into the NaCl solution or DMEM physiological medium solution was measured by atomic absorption spectrometry (Z5000 Polarized Zeeman Atomic Absorption Spectrophotometer, Hitachi Ltd., Tokyo, Japan), respectively, after 1, 4 and 24 h of shaking time. The calcium ions including those strongly bound to alginate molecules were extracted with DMEM medium in the presence of 0.1 M EDTA.

2.6 Cell culturing and hemolysis test of the wound dressings

All test samples were sterilized by UV light for 24 h before used for cell culturing or applied as wound dressing for animal implant study. For cell culturing, L929 mouse fibroblasts (5×10^4 cells) in 4 ml growth medium of DMEM/10% fetal calf serum were evenly seeded on the surface of a 6 cm-diameter Petri dish and then cultured in a humidified incubator at 37°C in air with 10% CO_2. On the 1st, 2nd, and 3rd days after seeding, the cells-containing samples were transferred to Eppendorff tubes and incubated with 0.5 mg/ml MTT at 37°C for 4 h. After that, the supernatants were centrifuged and DMSO was added followed by vigorous shaking to dissolve the purple formazan crystals formed. The absorbance was measured with a spectrophotometer (DU® series 600 UV/Vis spectrophotometer, Beckman Coulter, Inc., USA) at a wavelength of 570 nm.

For the hemolysis assay [15], the test wound dressing (100 mg) was equilibrated in saline solution (0.9% w/v NaCl) for 24 h. Then, 10 ml of 0.9% saline was added to each sample for 30 min at 37°C. To this solid/liquid suspension mixture, 0.2 ml dilute blood (anticoagulated SD rat blood was diluted with normal saline water according to volume ratio 1/1.25) was added, and then incubated for 60 min at 37°C. Negative and positive controls were obtained by adding 0.2 ml dilute blood to 10 ml saline solution and 0.1% Triton X-100 solution, respectively. After incubation, the solution was centrifuged at 2,500 rpm for 5 min and hemolytic activity was quantitated by using 96-well culture plates and measuring the absorbance of supernatant at 540 nm.

2.7 Animal implant study

Male Spague-Dawley rats of 7-week age with 250 ± 50 g body weight were obtained from the animal center of National Yang-Ming University. Prior to the test, the rats were anaesthetized with pentobarbital. Next, the dorsal hair of the rat was removed using an electric razor and a wound with a surface area of 3 × 3 cm^2 was created by excising the full-thickness of the dermis of the rat. It was then covered with one of the four dressings: Gauze, Kaltostat®, Type-AP and Type-AE, all of the same size as the created wound. Treated rats were placed in individual cages and wound tissues were dissected for observation at different healing time. On the 7th, 14th, 21st postoperative day, the dressings were removed and visual (macroscopic) inspections of the wounds on the rats (which were anesthetized) were conducted regarding to the appearance and size. The wound area (non-epidermized zone) was estimated by transposing the wound site onto a graph paper, and the surface area of each transfer was analyzed by planimetry on a MEDIA CYBERNETICS® analyzer (Optimas® Version 6.5, Media Cybernetics, Inc. USA). The healing rate was expressed by the wound-healing index defined as following:

$$\text{Wound-healing index} = \{\, \text{Aw\_0} - \text{Aw\_n} \} \,/\text{Aw\_0} * 100\% \,,$$

where A_{w_n}: the area of wound on the *n*th day, A_{w_0}: the area of wound created initially.

After the visual inspections for calculating the healing index, wound tissues were dissected, fixed with 10% phosphate-buffered formalin and stained with hematoxylin-eosin (H&E) reagent for histological observations.

2.8 Statistical analysis

Statistical analysis of the data comparison between the tested groups was conducted by one-way analysis of variance and determination of confidence intervals, using the *Statistical Analysis System* program, Version 6.08 (SAS Institute Inc., Cary, NC) and data was presented as mean ± SD.

3 Results

3.1 Reaction of alginate with PEI (or Ethylenediamine)

Figure 1 depicts the mechanism of carboxylic acid activation of alginate by EDC and its further reaction with amines (PEI or Ethylenediamine) to form the amide bonds in Type-AP and Type-AE dressings, respectively. The existence of the amide bonds is confirmed by the results of FTIR analysis.

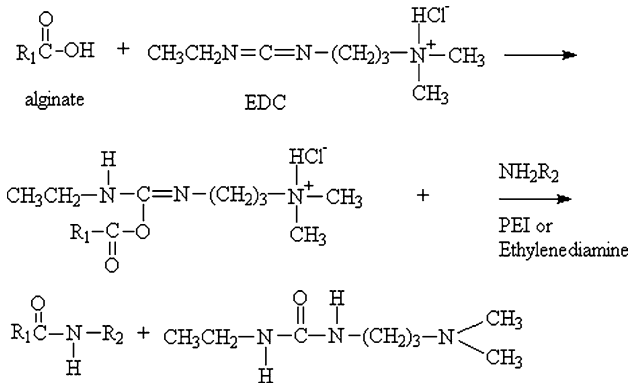

Fig. 1 Activation of the carboxylic group by EDC followed by reactions with amines to yield the amide linkage. (R_1COOH: alginate; NH_2R_2: PEI or Ethylenediamine)

FTIR spectra of both Type-AP and Type-AE dressings are presented in Fig. 2. For alginate, the absorption bands at 1,589 and 1,412 cm^{-1} were due to the respective asymmetric and symmetric stretching vibrations of carboxylate anions. The absorption band at 1,589 cm^{-1} shifted to 1,611 cm^{-1} after alginate reacted with the amines via crosslinking reaction of EDC. In addition, both Type-AP and Type-AE dressings had absorption band at 1,468 cm^{-1} due to the scissoring of the aliphatic hydrocarbon chain ($\delta_s CH_2$) of PEI and Ethylenediamine. Two specific peaks of the products (R_1CONHR_2) were seen in the FTIR spectra. The absorption at 1,668 cm^{-1} was attributed to the C=O bond whereas 1,561 cm^{-1} to the N–H bond. For Type-AP, the C=O absorption band might have overlapped with the primary anime of PEI, and was shown as a shoulder at around 1,668 cm^{-1}.

3.2 Microstructures of the wound dressings

Figure 3 shows the SEM images of the Kaltostat®, Type-AP and Type-AE dressings. As shown, Kaltostat® had a non-woven structure with fibers appeared to align in one direction (Fig. 3a), whereas both Type-AP and Type-AE dressings (Fig. 3b, c) displayed a sponge-like structure with average pore diameters of about 100–250 μm. Results of the EDS analysis (Table 1) indicated that both Type-AP and Type-AE dressings had around 15% of nitrogen content (from the amines of PEI and Ethylendiamine) in their compositions. Both Type-AP and Type-AE dressings had lower calcium content than the Kaltostat® dressing.

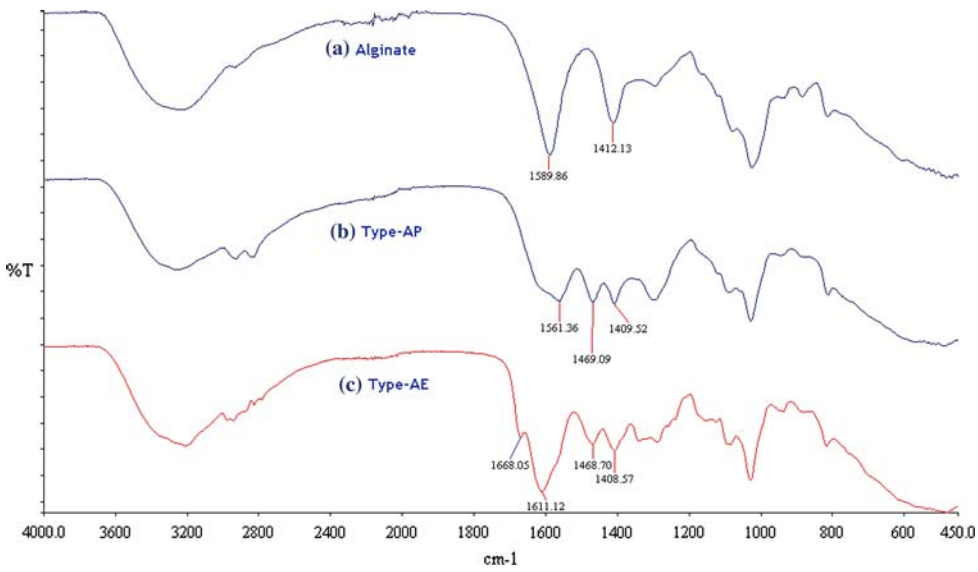

Fig. 2 FTIR spectra of (a) alginate, (b) Type-AP dressing, and (c) Type-AE dressing

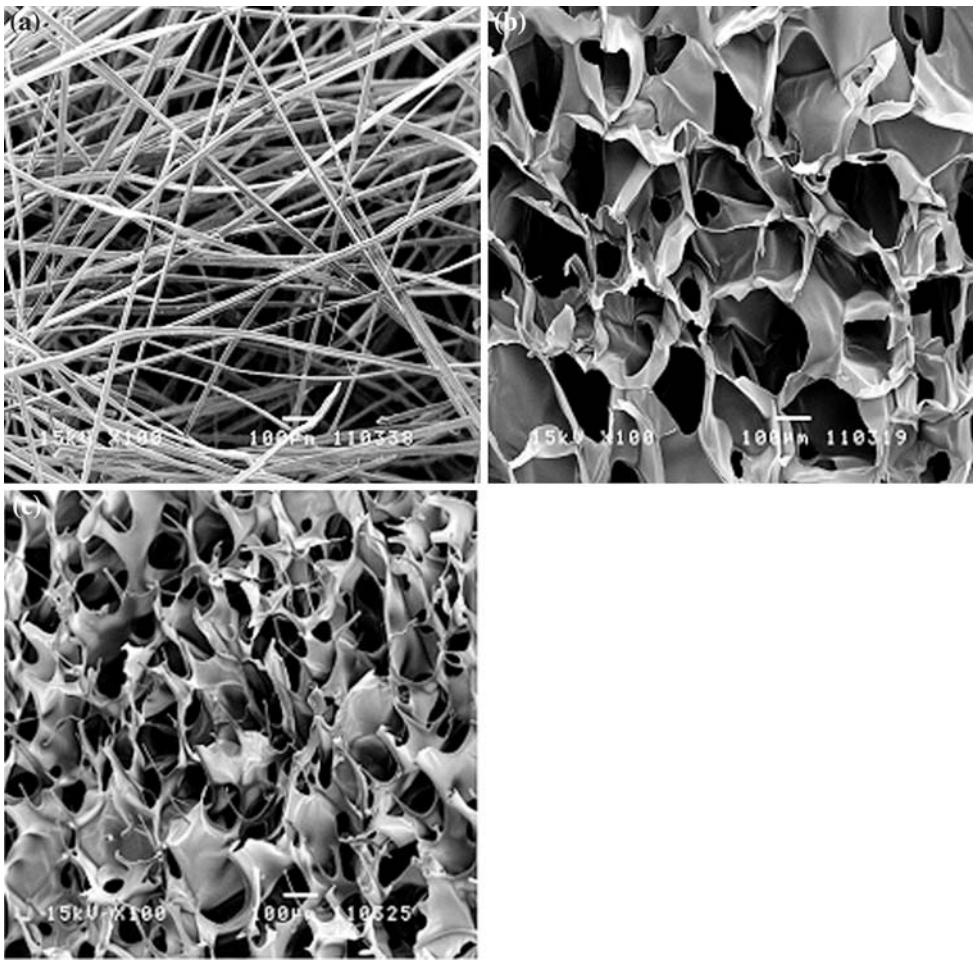

Fig. 3 SEM images of the (**a**) Kaltostat®, non-woven (×100); (**b**) Type-AP, sponge-like (×100), and (×) Type-AE (×100), sponge-like structures

Table 1 Surface element analyses (EDS) of the three alginate-based dressings

Atom (%)	Alginate-based dressings		
	Kaltostat®	Type-AP	Type-AE
C	41.66 ± 1.32	41.29 ± 0.70	49.79 ± 0.88
O	48.96 ± 2.10	38.54 ± 2.01	32.63 ± 1.22
N	–	14.60 ± 1.35	15.83 ± 0.54[a]
Ca	9.38 ± 0.78	3.58 ± 0.93	1.75 ± 0.39[b]

[a] No significant difference between Type-AP and Type-AE ($P > 0.05$)

[b] Significant difference among Kaltostat[R], Type-AP, and Type-AE ($P < 0.05$)

Mean ± SD ($n = 20$)

3.3 Physical properties of the wound dressings

After crosslinking reaction, both Type-AP and Type-AE dressings showed decreased water content and increased degradation temperature. Among the three dressings, Type-AP had the lowest water content (83 ± 0.4%) and the highest degradation temperature (190.3 ± 0.9°C) (Table 2).

The most prominent difference in physical properties among the three alginate-based dressings is their mechanical strengths. Because material was strengthen by crosslinking reaction, much higher values of ultimate tensile strength and tensile modulus were seen in Type-AP (12.37 ± 1.72 MPa/25.15 ± 1.79 MPa) and Type-AE (6.87 ± 0.5 MPa/19.16 ± 1.38 MPa) dressings as compared with Kalostat® (0.87 ± 0.12 MPa/1.2 ± 0.19 MPa).

The water vapor perambilities of both Type-AP and Type-AE dressings were about 3,500 g/m^2/day, higher than the 2,538 g/m^2/day for Kaltostat®. These values are in the range of WVTRs of the normal skin (∼204 g/m^2/day) and injured skins (ranging from 279 g/m^2/day for a first-degree burn to 5,138 g/m^2/day for a granulating wound) [13].

In this study, the unreacted residual ethylenediamine of Type-AE dressing was measured by ninhydrin assay. The result shows one gram Type-AE contains 8.5 ± 0.6 mg residual ethylenediamine (Mean ± STD, $n = 8$). This is about 20% of the ethylenediamine (43.6 mg) initially blended with alginate for preparing the Type-AE dressing.

Table 2 Physical and chemical properties of the three alginate-based dressings

Physical and chemical properties	Alginate-based dressings		
	Kaltostat®	Type-AP	Type-AE
WVTR (g/m^2/day)	2538 ± 150[a]	3556 ± 39[b]	3561 ± 74
Water content (%)	82.52 ± 0.43[a]	86.96 ± 0.72[c]	88.77 ± 0.59
Degradation temperature (°C)	180.45 ± 0.26[a]	190.26 ± 0.88[c]	182.62 ± 0.97
Maximum stress (MPa)	0.87 ± 0.12[a]	12.37 ± 1.72[c]	6.87 ± 0.50
Young's modulus (MPa)	1.30 ± 0.19[a]	25.15 ± 1.79[c]	19.16 ± 1.38
Elongation at fracture (%)	10.79 ± 0.42	9.96 ± 0.60[c]	7.14 ± 0.68

WVTR: water vapor transmission rate

[a] Significant difference between Kaltostat® and crosslinked groups (Type-AP and Type-AE) ($P < 0.05$)

[b] Significant difference between Type-AP and Type-AE ($P < 0.05$)

[c] No significant difference between Type-AP and Type-AE ($P > 0.05$)

Mean ± SD ($n = 5$)

3.4 The content of calcium ions

Figure 4 shows the amount of calcium ions released into the 0.9% NaCl solution or DMEM medium solution from the test dressings. Among three test dressings, Kalostat® has the highest calcium ions content, followed by Type-AP and subsequently Type-AE. The crosslinked Type-AP and Type-AE dressings showed a lower calcium ion release rates than the Kalostat® dressing. There is also a significant difference in calcium ion release rates between the two crosslinked Type-AP and Type-AE dressings. This could be explained partially by the denser microstructure of Type-AE matrix as compared with that of Type-AP (Fig. 3). The release of calcium ions into DMEM medium appeared to be higher than that into 0.9% NaCl solution. Furthermore, the extraction of some strong bound calcium ions requires the action of chelating agent EDTA.

3.5 Cell culturing with the wound dressing materials

The biocompatibility of the two alginate-based dressings were demonstrated by culturing L929 fibroblast cells on these substrates. As shown in Fig. 5, fibroblasts proliferated at a higher growth rate on the materials of Type-AP and Type-AE than those cultured on Kalostat® dressing. On day 3 after cells seeding, the L929 fibroblasts on the surface of the fabricated dressings showed well-spread,

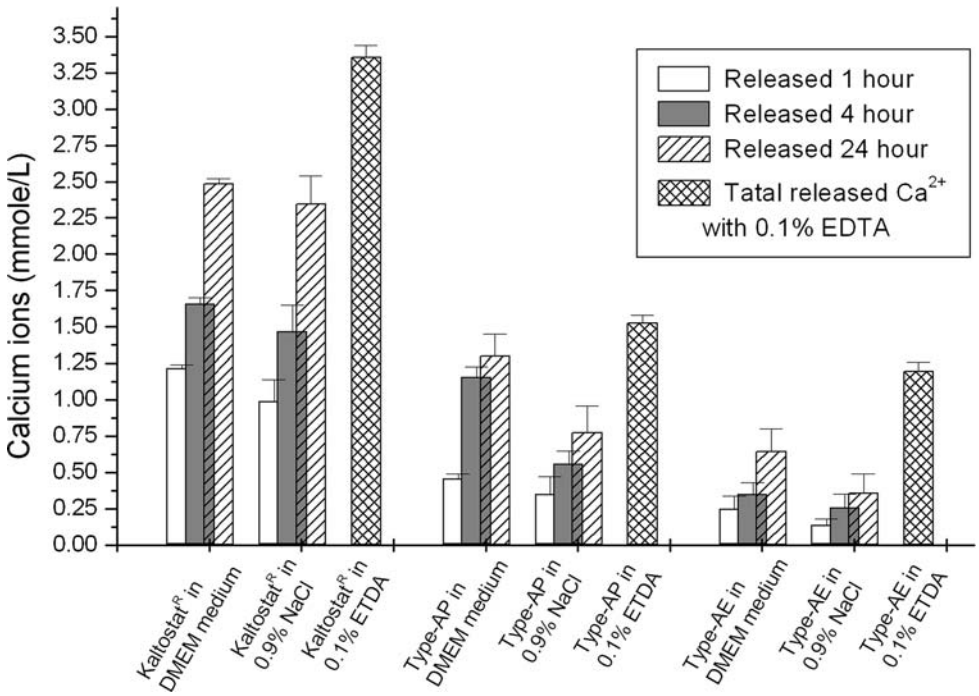

Fig. 4 The calcium ions released from Kaltostat®, Type-AP, and Type-AE dressings into the immersing solution at different time. (Mean ± SD, $n = 5$)

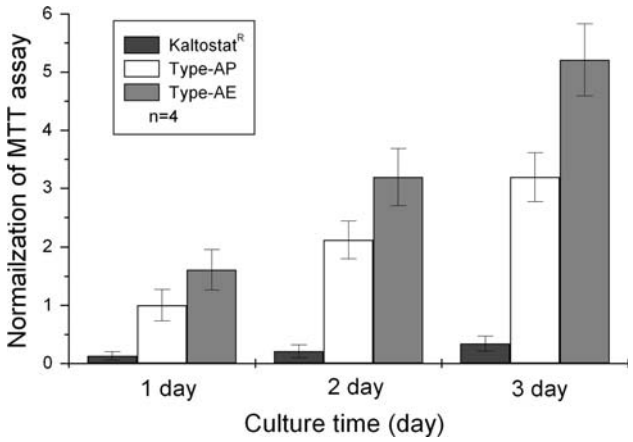

Fig. 5 The activities of L929 fibroblasts (FB) cultivated on the Kaltostat® (■), Type-AP (□), and Type-AE (■) dressings. Data are normalized to the control group, which is defined as the absorbance of the MTT assay of the FB cultivated on Type-AP dressing on the 1st day. The initial cell number was 2×10^4 (cells per well). (Mean ± SD, $n = 4$)

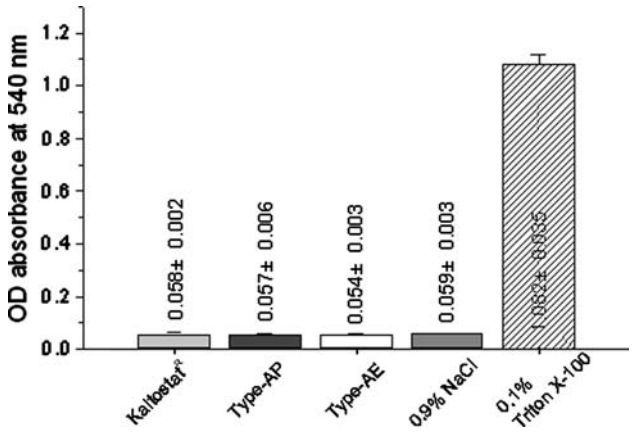

Fig. 7 Hemolytic activity of Kaltostat®, Type-AP and Type-AE. The solutions of 0.9% NaCl and 0.1% Triton X-100 were used as the negative and positive control agents, respectively, in inducing hemolytic reaction. (Mean ± SD, $n = 6$)

spindle shape with filopodia extended onto the matrix (Fig. 6). The adherent cells attached and grew well on the newly developed dressings of Type-AP and Type-AE. In addition, all test dressings, when contacted with rat red blood, did not cause any significant hemolysis (Fig. 7).

3.6 Wound healing performance

For all three alginate-based dressings tested, there was no tissue fluid accumulated between the dressings and the injured tissues covered underneath, and the dressings were in a moist state around the wounds. Based on the macroscopic observation all three dressings appeared to be capable of absorbing the tissue exudates and were of a suitable permeability of body fluid in consistency with their WVTR measured in vitro.

Replacement of the implanted alginate-based dressing with a new one did not present any problem as the membrane could be easily separated from the healing wound of skin. While gauze often adhered to the re-generated tissue (Figs. 8a and 9a), the alginate-based dressing turned into a moist-state material at the dressing/wound interface after being left on the wound site for 7 and the 21 days after operation (Fig. 8b–d). This moist-state material did not adhere to the re-generated tissue and could be removed easily by saline washing at the wound. The cleaned wound, pink in color, could be seen during the healing process. New epidermis grew out from the margin to the center of the wound, and the depth and size of the wound gradually reduced with time. The healing rate across the wound in the transverse (waist) direction of the wound site was faster than that in the longitudinal (vertebral direction). Therefore, the shape of the healing wound became rectangular, and more and more slender with time as shown by Fig. 9.

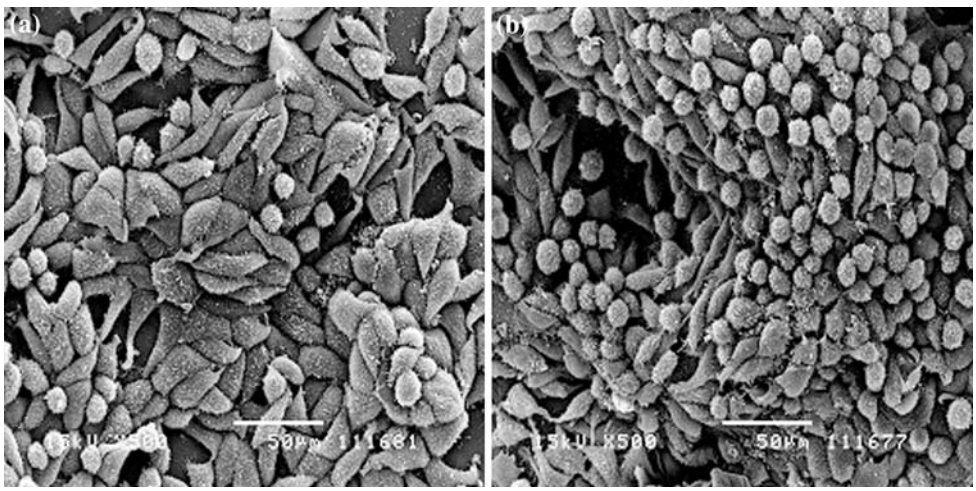

Fig. 6 SEM photographs of L929 fibroblasts (FB) grew and attached on (**a**) Type-AP and (**b**) Type-AE dressings (3 days after seeding) under 500× magnifications. The cell exhibits a typical spindle-shape of FB on the surface of dressing. Note that the FB has developed extended and overlapping filopodias. The initial cells density of FB was adjuster to 2×10^4 and seeded on the 1 cm-diameter dressing

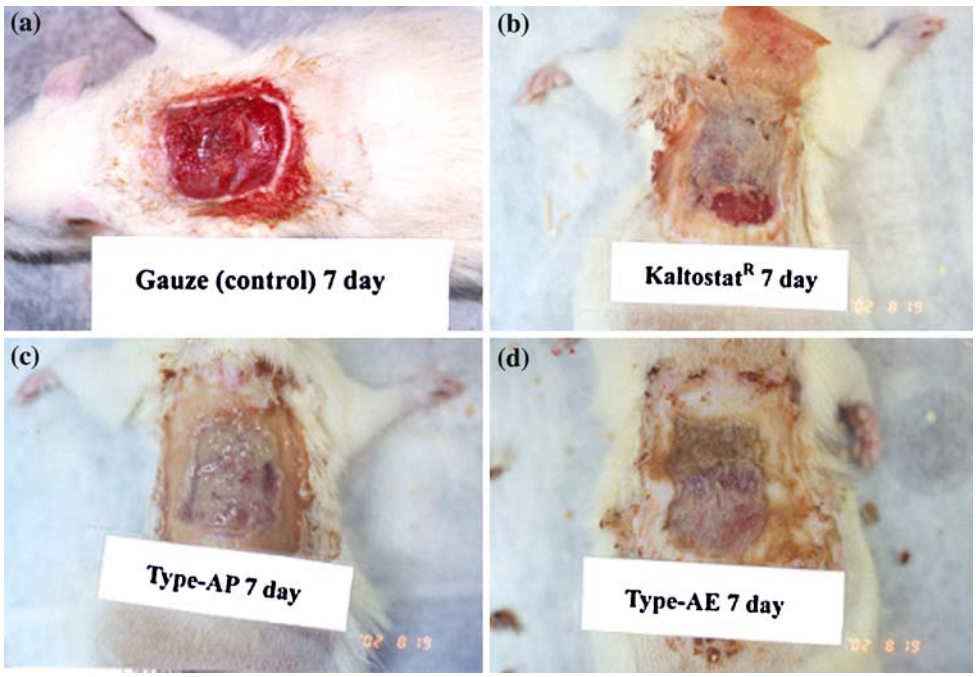

Fig. 8 Photographs of the wounds on the 7th day after operation treated respectively with the four different dressings (**a**) Gauze (control), (**b**) Kaltostat®, (**c**) Type-AP, and (**d**) Type-AE

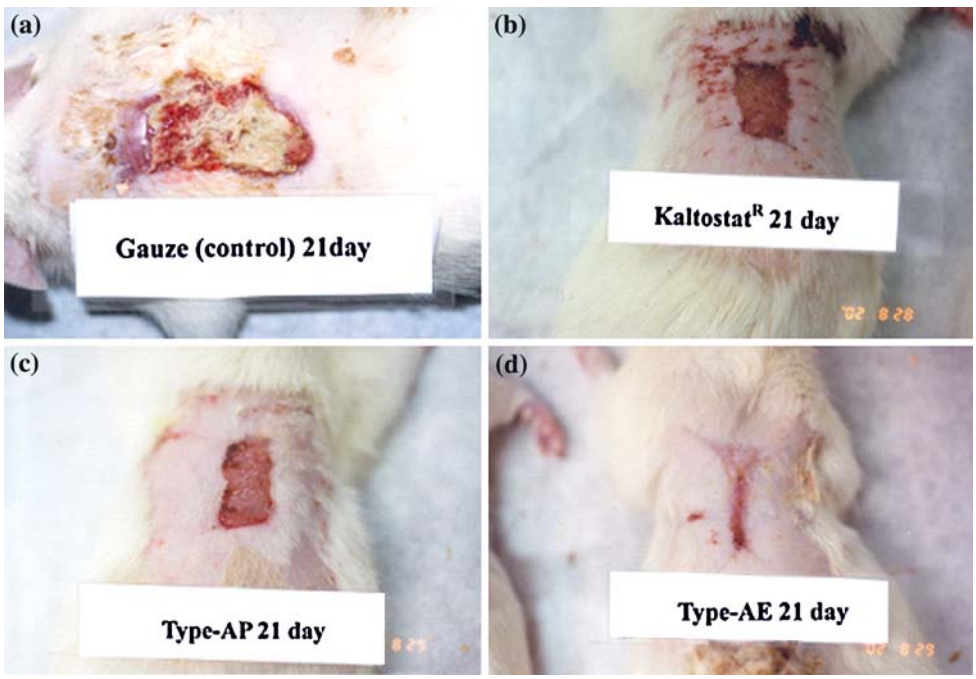

Fig. 9 Photographs of the wounds on the 21th day after operation treated respectively with the four different dressings (**a**) Gauze (control), (**b**) Kaltostat®, (**c**) Type-AP, and (**d**) Type-AE

The performance of the different dressings was compared using the wound-healing index as shown in Fig. 10. For the control case, the adhesion of gauze to the wound tissue caused great difficulty in the estimation of wound-healing index. Overall, gauze had a negative effect on wound healing due to the severe wound tissue adhesion. On the other hand, the three cases of the wounds covered with the alginate-based dressings healed at about the same rate in the first week after implantation. However, on the 14th day and the 21st day, the Type-AE sponge appeared to have significantly higher wound-healing index value ($P < 0.05$) than the other two. Overall, Type-AP and Type-AE were superior to the commercial Kalostat®.

3.7 Histopathology of the wound healing

During the skin wound regeneration, epithelial cells (dark brown color with H&E stain) proliferated progressively from the edge to the center of the wound site (Fig. 11). The epithelial layer of the regenerated wound site outgrew from

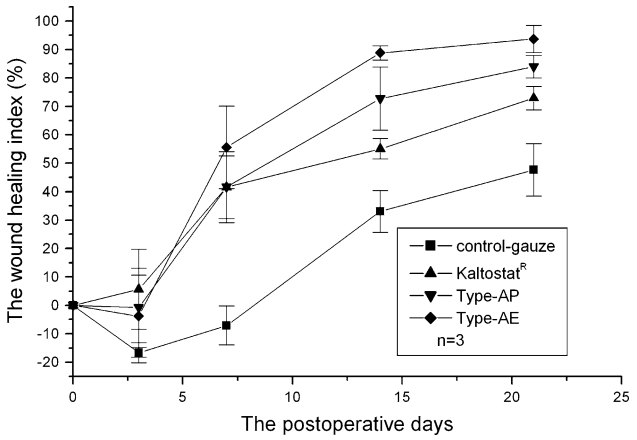

Fig. 10 The healing indices of wounds treated with the four different dressings: Gauze (control; ■), Kaltostat® (▲), Type-AP (▼), and Type-AE (◆). (Mean ± SD, $n = 3$)

the surrounding undamaged skin as indicated by the boundary in Fig. 11 (dot-line). In the cases of gauze and Kaltostat® dressings, the graft materials were encapsulated in the granulation tissues of the wound sites in the early stage (7th days; Fig. 11a, b) and they appeared to affect the advancement of epithelial layers. Both the newly formed epithelium (solid-line arrows in Fig. 12) and the residual materials (dotted-arrows in Fig. 11a, b) could be located in the wound sites. For both Type-AP and Type-AE dressings, epithelial layers covered almost all surface area of the wound sites (Fig. 11c, d) 21 days after operation. On the other hand, encapsulation of dressing materials by fibroblasts in the granulation tissue (dotted-line arrow) was still seen for gauze (Fig. 12a) and Kaltostat® (Fig. 12b) on the 21st day after operation. Blood capillaries (solid-line arrow) were found in the newly formed tissue treated with skin grafts, especially in the wound sites covered with Type-AE dressing. These results combined with the calculated wound-healing index showed that both Type-AP and Type-AE dressings were of higher-than-expectation efficacy in treating skin wounds than the commercial one.

4 Discussion

In this study, both Type-AP and Type-AE dressings had higher mechanical strength and degradation temperature but lower calcium content and calcium ion release rate as compared with the commercial Kaltostat® dressing. The two newly developed sponge-type dressings fabricated for this study had WVTR of 3,500 g/m^2/day higher than the 2,538 g/m^2/day of Kaltostat®. The differences in WVTR could be attributed to the differences in both chemical compositions and physical structures. Although Type-AP and Type-AE dressings had higher WVTR they still maintained an adequate level of moisture to prevent the dehydration of the wounds.

In this study, we have found that Type-AP dressing has both higher mechanical strength and higher degradation temperature than Type-AE dressing. This could be attributed to that the branched PEI crosslinked with alginate at multiple sites along the same macromolecule which provide Type-AP dressing a more stable structure. On the other hand, although ethylenediamine has only two coupling site

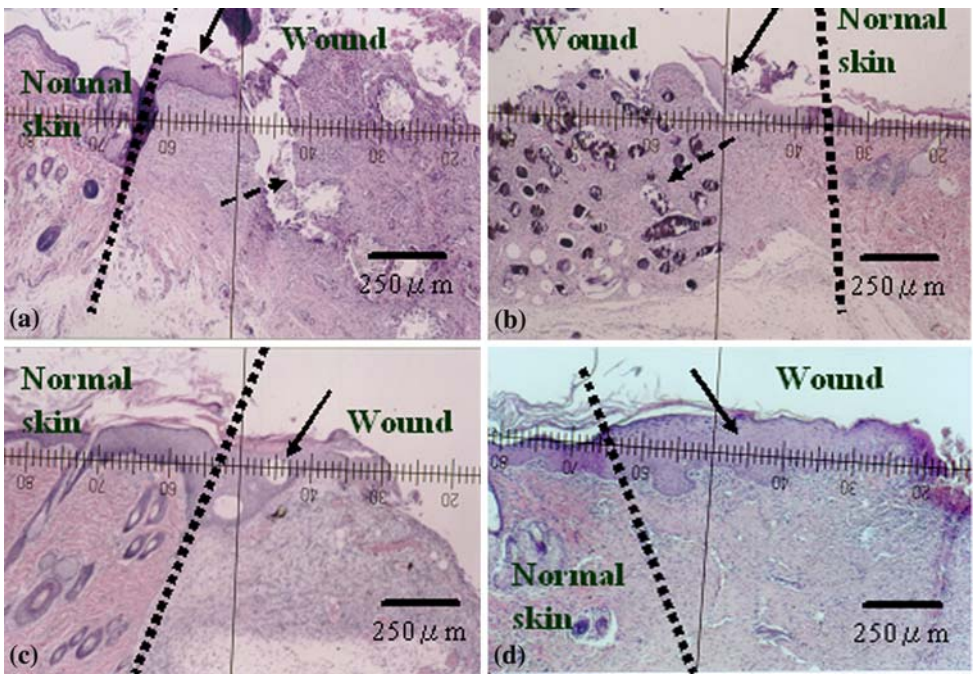

Fig. 11 Histological section of the skin wounds with H&E stain on the 7th day after operation treated with the four different dressings: (**a**) Gauze (control), (**b**) Kaltostat®, (**c**) Type-AP, and (**d**) Type-AE. (dotted lines: boundary between normal skin and wound skin; solid arrow: newly grown epithelium; dotted arrows: material encapsulated in granulation tissue)

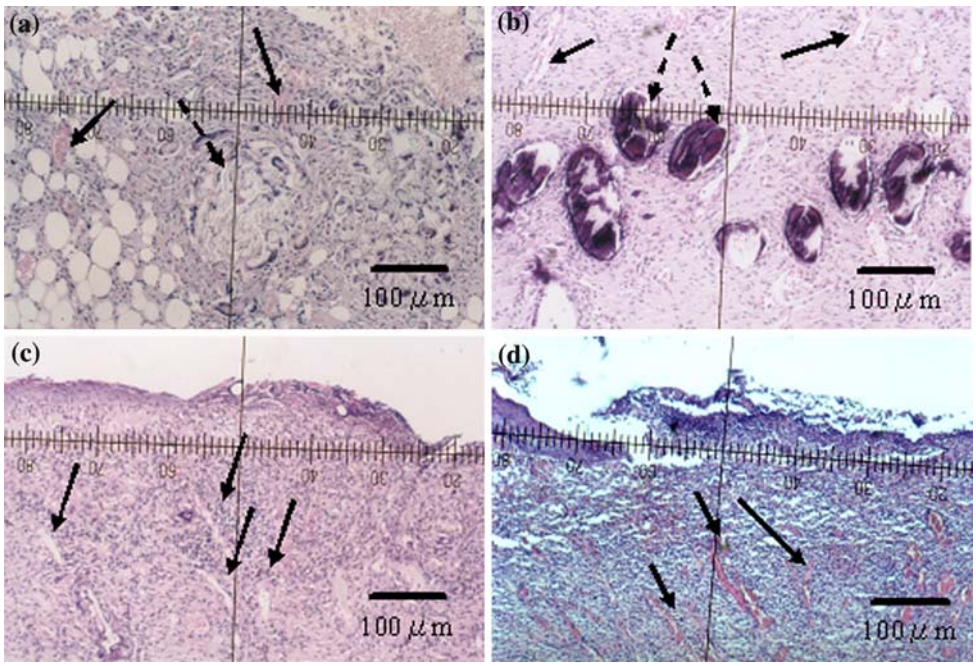

Fig. 12 Histological section of the skin wounds with H&E stain on the 21th day after operation treated with the four different dressings: (**a**) Gauze (control), (**b**) Kaltostat®, (**c**) Type-AP, and (**d**) Type-AE. (Solid arrow: newly grown blood capillaries; dotted arrows: material encapsulated in granulation tissue)

at the most to react with alginate, but this small molecule can penetrate more freely inside the alginate matrix. This might explain why more amine groups ($-NH_2$) of Type-AE were consumed as compared with that of Type-AP. This resulted in a higher unreacted carboxyl groups (–COOH) remained in Type-AP and also higher calcium ions content of Type-AP as compared with Type-AE.

Calcium ions were rapidly released from calcium alginate gel in exchange for sodium ions when the dressing came in contact with blood [16]. High concentration of calcium ion (10 mmol/l) was reported to inhibit the growth of cells in culture [17, 18], and the extraction media from calcium alginate gel induced cytopathic effects on both fibroblasts and epidermal cells [19]. Among the three alginate-based dressings in this study, Type-AE dressing had the lowest calcium content (Table 1) and the lowest calcium ion releasing rate (0.36 ± 0.13 mmol/l in 0.9% NaCl and 0.65 ± 0.15 mmol/l in DMEM medium, the 24 h after operation) as well (Fig. 4). This explains in part that Type-AE dressing has a significantly higher skin wound healing index value than the other two alginate-based dressings.

It has been reported that wounds re-epithelialized more rapidly under moist conditions [20]. Moist-state material, which covers the wound, absorbs the exudates and keeps the wound naturally and suitably moist. Both Type-AE and Type-AP dressings as well as the commercial Kalostat® dressing were in moist-state in the early stage of skin wound healing, but fibrous tissue encapsulates the debris of the commercial Kaltostat® (Figs. 11b and 12b) in the late stage of wound healing. The Type-AP and Type-AE dressings, on the other hand, did not result in the formation of encapsulated alginate-based materials during skin wound healing process (Figs. 11c, d and 12c, d). This indicates that the new dressings developed in this study is more advantageous than the commercial counterpart since the encapsulated alginate-based materials was reported to hinder wound healing [21, 22]. The retardation in wound closure and the subsequent higher risk of reacting with foreign materials could potentially induce undesirable complications such as the formation of hypertrophic scar and keloid [23].

5 Conclusion

In this study, we have developed two alginate-based wound dressings, Type-AP and Type-AE, with macroporous sponge-liked structure with lower calcium content, better heat stability and higher mechanical strength and lower calcium ion release rate as compared with Kaltostat®. We have further demonstrated that the fabricated dressings had higher skin wound-healing index, and therefore were superior materials for wound dressings than Kaltostat®.

References

1. M. Chvapil, J. Biomed. Mater. Res. **11**, 721 (1977)
2. L.H.H. Olde Damink, P.J. Dijkstra, M.J.A. Van Luyn, P.B. Van Wachem P. Nieuwenhuis, J. Feijen, J. Biomed. Mater. Res. **29**, 149 (1995)
3. S.M. Kuo, S.W. Tsai, L.H. Huang, Y.J. Wang, Artif. Cells Blood Substit. Immobil. Biotechnol. **25**, 551 (1997)
4. T. Gilchrist, A.M. Martin, Biomaterials **4**, 317 (1983)
5. G.T. Grant, E.R. Morris, D.A. Rees, P.J.C. Smith, D. Thom, FEBS Lett. **32**, 195 (1973)

6. H. Zheng, Carbohydr. Res. **302**, 97 (1997)
7. S.J. Chang, C.H. Lee, C.Y. Hsu, Y.J. Wang, J. Biomed. Mater. Res. **59**, 118 (2002)
8. L. Shapiro, S. Cohen, Biomaterials **18**, 583 (1997)
9. S.J. Seo, Y.J. Choi, T. Akaike, A. Higuchi, C.S. Cho, Tissue Eng. **12**, 33 (2006)
10. S.J. Seo, I.Y. Kim, Y.J. Choi, T. Akaike, C.S. Cho, Biomaterials **27**, 1487 (2006)
11. Y.S. Choi, S.R. Hong, Y.M. Lee, K.W. Song, M.H. Park, Y.S. Nam, Biomaterials **20**, 409 (1999)
12. B. Balakrishnan, M. Mohanty, P.R. Umashankar, A. Jayakrishnan, Biomaterials **26**, 6335 (2005)
13. L. Ruiz-Cardona, Y.D. Sanzgiri, L.M. Benedetti, V.J. Stella, E.M. Topp, Biomaterials **16**, 1639 (1995)
14. H.W. Sung, Y. Chang, C.T. Chiu, C.N. Chen, H.C. Liang, J. Biomed. Mater. Res. **47**, 116 (1999)
15. D. Fisher, Y. Li, B. Ahlemeyer, J. Krieglstein, T. Kissel, Biomaterials **24**, 1121 (2003)
16. J.R. Fry, Pharmacol. J. **12**, 37 (1986)
17. C. Marchese, J. Rubin, D. Ron, A. Faggioni, M.R. Torrisi, A. Messina, L. Frati, S.A. Aaronson, J. Cell Physiol. **144**, 326 (1990)
18. A. Sank, M. Chi, T. Shima, R. Reich, G.R. Martin, Surgery **106**, 1141 (1989)
19. M. Rosdy, L.C. Clauss, J. Biomed. Mater. Res. **24**, 363 (1990)
20. C.D. Hinman, H. Maibach, Nature **200**, 377 (1963)
21. I.R. Matthew, R.M. Browne, J.W. Frame, B.G. Millar, Biomaterials **16**, 275 (1995)
22. E.W. Odell, P. Oades, T. Lombardi, Br. J. Oral. Maxillofac. Surg. **32**, 178 (1994)
23. Y. Suzuki, Y. Nishimura, M. Tanihara, K. Suzuki, T. Nakamura, Y. Shimizu, Y. Yamawaki, Y. Kakimaru, J. Biomed. Mater. Res. **39**, 317 (1998)